

Ab initio tight-binding Models for Mono- and Bilayer Hexagonal Boron Nitride (*h*-BN)

Srivani Javvaji,¹ Fengping Li,¹ and Jeil Jung^{1,2,*}

¹Department of Physics, University of Seoul, Seoul 02504, Korea

²Department of Smart Cities, University of Seoul, Seoul 02504, Korea

Hexagonal boron nitride (*h*-BN) exhibits dominant π -bands near the Fermi level, similar to graphene. However, unlike graphene, where tight-binding (TB) models accurately reproduce band edges near the K and K' points in the Brillouin zone, a wider bandgap in *h*-BN necessitates capturing the band edges at both the K and M points for precise bandgap calculations. We present effective TB models derived from *ab initio* calculations using maximally localized Wannier functions (MLWFs) centered on boron and nitrogen sites. These models consider hopping terms of up to four distant neighbors and achieve excellent agreement with *ab initio* results near the K and M points. Furthermore, we compare the band structures from our simplified models with those obtained from *ab initio* calculations and the full tight-binding model to assess their accuracy. To account for the effects of strains, we introduce fitting parametrizations that relate the hopping parameters of the effective TB model to the lattice constant and interlayer distance. Additionally, we utilize the two-center approximation to calculate the interlayer hopping energies based on the relative distances between sublattices to generalize the interlayer hopping parameters across different stacking configurations. We demonstrate the effectiveness of this method by comparing the electronic structure of zero-twist and twisted *h*-BN systems with *ab initio* calculations.

I. INTRODUCTION

Using *h*-BN as a two-dimensional substrate for graphene systems is prevalent in emerging electronic devices [1], moreover the resulting lattice mismatch and misorientation create moiré patterns that influence electronic properties [2–4]. Interestingly, twisted *h*-BN bilayers themselves exhibit unique electronic properties like flat bands, excitons, and strong correlations, making them intriguing systems, particularly due to their inherent bandgap [5–7]. Similar to graphene, *h*-BN features are dominated by π -bands near the Fermi level, which arise from the π -electrons in the p_z orbitals of boron and nitrogen atoms. The overlap of these p_z orbitals is crucial for constructing TB models for both *h*-BN monolayers and bilayers. However, existing TB parametrizations struggle to accurately reproduce the π -band dispersion across the entire Brillouin zone, particularly away from the K -point. While these models successfully capture the band edges near the K and K' points using methods such as *ab initio*-fitted minimal TB models [8–12] or K/K' -based continuum Hamiltonians [13], they often fail to accurately replicate the band structure around the M point and the dispersion throughout the Brillouin zone. This limitation complicates the precise estimation of the bandgap and its nature (direct or indirect), which is crucial for various device applications.

In this paper, we propose simplified TB models for monolayer and bilayer *h*-BN that consider only a limited number of distant neighbors. Despite the reduced complexity, our models accurately reproduce the band edges from density functional theory (DFT) calculations near high-symmetry points across the entire first Brillouin zone (FBZ). This allows for precise estimation of the bandgap and its characteristics in *h*-BN systems. We provide the necessary hopping parameters for constructing the model Hamiltonians for the monolayer and bilayer configurations examined in this study, and demon-

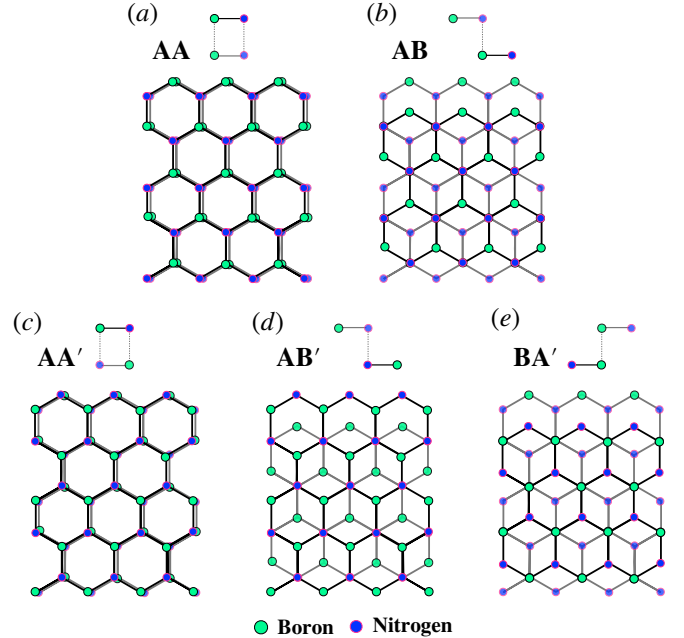


FIG. 1. (Color online) Top views of the *h*-BN bilayers with standard stacking configurations: a) AA, b) AB, c) AA', d) AB' and e) BA'. Green and blue circles represent boron and nitrogen atoms, respectively. Side views of each stacking is shown at the top of each sub-figure.

strate their effectiveness by comparing them with DFT band structure calculations. Additionally, we present effective hopping terms for modeling *h*-BN bilayers under various conditions, with fitting parameters based on interlayer distance and lattice parameters. We also introduce a generalized two-center approximation to map interlayer hopping in both zero-twist and twisted bilayers, while using our models to accurately describe intra-layer interactions.

The manuscript is organized as follows: In Section II, we provide a brief summary of the *ab initio* calculations used

* jeiljung@uos.ac.kr

in the study. In Section III, we present several TB model approximations to the first-principles-calculated band structures, and we provide the hopping parameters necessary to construct effective models. In Section IV, we present the revised two-center TB model for bilayer *h*-BN, and in Section V we present the conclusions of our findings.

II. AB INITIO CALCULATION DETAILS

We use the Quantum ESPRESSO package [14, 15] for all our first-principles calculations, employing a plane-wave basis set [16] within the local-density approximation (LDA) using the Perdew-Zunger parametrization [17]. For enhanced accuracy, we performed DFT calculations with a $42 \times 42 \times 1$ *k*-point sampling density and a plane wave cutoff energy of 60 Ry. We constructed the *h*-BN monolayer and bilayer structures using an LDA-DFT optimized lattice constant of $a = 2.48$ Å, which is slightly smaller than the experimental value of 2.504 Å [18].

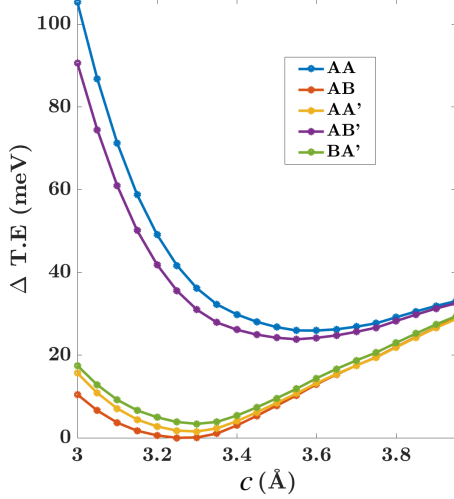


FIG. 2. (Color online) The total energy differences of various BLBN stackings are plotted against interlayer distance, relative to the most stable AB-stacking configuration at its equilibrium interlayer distance of $c = 3.261$ Å. The calculations were performed using DFT within the LDA.

The *h*-BN bilayers can exist in five distinct stacking configurations [9–12, 19–22], as shown in Fig. 1. These stacking arrangements influence the equilibrium distance between the layers, as evident from the variation in total energy with interlayer spacing (*c*) in Fig. 2. It is noted that AB-stacking is energetically stable compared to rest of the configurations [19–22], followed by the AA'-stacking with a total energy difference of 1.664 meV per unit cell, which benefits from attractive electrostatic interactions between vertically alternating boron and nitrogen atoms [19–22]. Since the most stable AB-stacked bilayer has an equilibrium interlayer distance of $c = 3.261$ Å (Fig. 2), we use this distance for all other stacking configurations when constructing the TB models. The

TB Hamiltonian matrix elements are obtained by transforming the DFT Hamiltonian from the Bloch basis to the Wannier basis. This process involves first determining the electronic structure through DFT calculations. Subsequently, Wannier functions are generated from a set of localized orbitals centered at boron and nitrogen atoms using WANNIER90 [23]. The transformation is then facilitated by overlap matrices between Bloch states and Wannier functions, computed within the WANNIER90 [23] tool. This process directly provides the TB parameters: on-site energies from diagonal elements and hopping integrals from off-diagonal elements. This approach builds upon previous work developing a full tight-binding (FTB) model for both monolayer and bilayer graphene, which accurately reproduced low-energy bands from first-principles LDA calculations [24, 25].

III. TIGHT-BINDING MODELS

A. Hamiltonian

The Hamiltonian for the π -bands in BLBN can be represented by a \mathbf{k} dependent 4×4 size matrix:

$$H_{\text{BLBN}}(\mathbf{k}) = \begin{pmatrix} H_{\text{MBN}_1}(\mathbf{k}) & H_{\text{Coupl}}(\mathbf{k}) \\ H_{\text{Coupl}}^\dagger(\mathbf{k}) & H_{\text{MBN}_2}(\mathbf{k}) \end{pmatrix} \quad (1)$$

where $H_{\text{MBN}_1}(\mathbf{k})$ and $H_{\text{MBN}_2}(\mathbf{k})$ are 2×2 size Hamiltonian matrices that describe the inter- and intra-sublattice hopping processes within each layer. These matrices are given by:

$$H_{\text{MBN}_i}(\mathbf{k}) = \begin{pmatrix} H_{\text{B}_i\text{B}_i}(\mathbf{k}) & H_{\text{B}_i\text{N}_i}(\mathbf{k}) \\ H_{\text{N}_i\text{B}_i}(\mathbf{k}) & H_{\text{N}_i\text{N}_i}(\mathbf{k}) \end{pmatrix} \quad (2)$$

where $i = 1, 2$ denotes the indices for the top and bottom layers, respectively. The coupling between these two layers is described by:

$$H_{\text{Coupl}}(\mathbf{k}) = \begin{pmatrix} H_{\text{B}_1\text{B}_2}(\mathbf{k}) & H_{\text{B}_1\text{N}_2}(\mathbf{k}) \\ H_{\text{N}_1\text{B}_2}(\mathbf{k}) & H_{\text{N}_1\text{N}_2}(\mathbf{k}) \end{pmatrix} \quad (3)$$

Each element of the Hamiltonian matrix, representing hopping processes between a distinct pair of atomic orbitals, is defined as a sum over neighbor indices *n*, as shown below:

$$H_{\alpha\beta}(\mathbf{k}) = \sum_n t_n e^{i\mathbf{k} \cdot \mathbf{R}_n} \quad (4)$$

Here, t_n signifies the hopping energy, and \mathbf{R}_n denotes the position vector describing the hopping process between sublattices α and β , which consist of boron or nitrogen atoms. The summation over the phase factor $e^{i\mathbf{k} \cdot \mathbf{R}_n}$ is known as the structure factor, accounting for the arrangement of the n^{th} neighbors [24, 25]. This is denoted by $g_n(\mathbf{k})$ and $f_n(\mathbf{k})$ for the intra- and inter-sublattice hopping processes, respectively. For simplicity we will denote these structure factors as G_n and F_n in this paper.

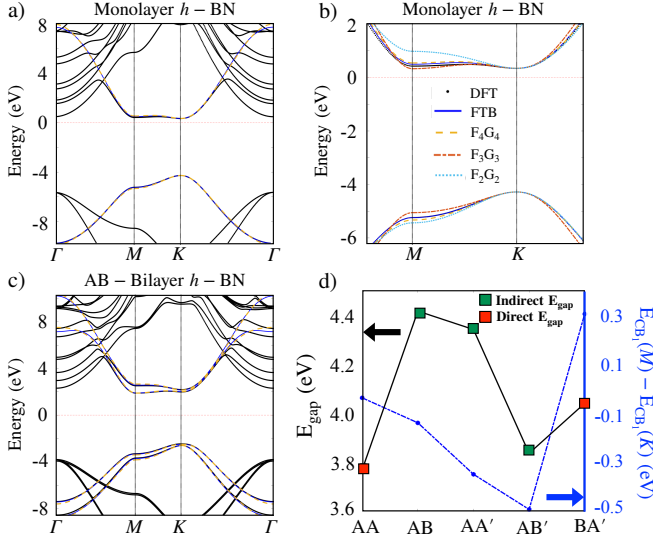


FIG. 3. (Color online) Band structures for (a) MBN and (c) AB-stacked BLBN are shown across the high-symmetry points in the FBZ. The results are obtained from DFT and compared with the FTB and the simpler effective TB (F_2G_2 , F_3G_3 & F_4G_4) models with fewer parameters. (b) For MBN, the FTB & F_4G_4 models demonstrate superior agreement with *ab initio* calculations near the K-point and M-point compared to F_2G_2 and F_3G_3 . (d) The primary bandgap (E_{gap}) obtained from DFT for all five stacking types in BLBN is shown by the black line. The direct and indirect bandgap nature is indicated by red and green rectangles, respectively. The dashed blue line represents the energy difference between the primary conduction band minimum at the M-point and at the K-point for each stacking configuration.

The FTB model Hamiltonian is constructed by considering up to $n = 15$ neighbors for each element as described in Eq.(4). To reduce the complexity we build simpler effective TB models that only consider a limited number of nearest neighbors. These models are derived from the low-energy $\mathbf{k} \cdot \mathbf{p}$ Hamiltonian, which is obtained by performing a Taylor expansion of the energy bands around the K-point [24, 25]. In this $\mathbf{k} \cdot \mathbf{p}$ framework, the Hamiltonian element $H_{\alpha\beta}(\mathbf{k})$ is computed by expanding the bands at $\mathbf{k} = \mathbf{k}_D + \mathbf{k}$, where \mathbf{k}_D is the K-point and \mathbf{k} is a small deviation vector. The details of this expansion are provided in Appendix A. This expansion decomposes $H_{\alpha\beta}(\mathbf{k})$ into two components, diagonal elements ($\alpha = \beta$) corresponding to intra-sublattice processes (see Eq. A1) and off-diagonal elements ($\alpha \neq \beta$) representing inter-sublattice processes (see Eq. A2). The zeroth-order expansion coefficient, $C'_{\alpha\beta 0}$, governing intra-sublattice processes, and the first-order coefficient, $C_{\alpha\beta 1}$, for inter-sublattice processes are essential for constructing the effective Hamiltonian. These coefficients are derived from the hopping parameters, as expressed in Eqs. A3 and A4 [24].

B. Bandstructures

We present the electronic band structures calculated for the MBN and BLBN systems using both the FTB and effective models. Fig. 3 compares the band structures of h-BN monolayer and the most stable AB stacked bilayer, obtained from DFT, the FTB model, and simplified effective models incorporating up to $n = 2, 3$, and 4 nearest neighbors. The FTB model accurately reproduces the band edges at the K and M points, as well as the overall band behavior across the FBZ. However, for simpler calculations, we developed effective TB models that capture these key band edge features. Starting with the double structure factor model, F_2G_2 , truncates the G_n and F_n functions at $n = 2$. In this model, the nearest neighbor hopping terms are taken from *ab initio* hopping data, while the more distant ($n = 2$) terms are corrected using expressions derived from the coefficients in Eqs. A3 and A4, as detailed in previous studies [24, 25]:

$$\begin{aligned} t_{\alpha\beta 2} &= C_{\alpha\beta 1}/\sqrt{3}a + t_{\alpha\beta 1}/2, \\ t'_{\alpha\beta 2} &= \frac{1}{6}(C'_{\alpha\beta 0} - t'_{\alpha\beta 0} + 3t'_{\alpha\beta 1}). \end{aligned} \quad (5)$$

Here, $t'_{\alpha\beta n}$ represents the hopping energy of the n^{th} nearest neighbor hopping process from sublattice α to β , where the primes indicate expansions of the G_n structure factor terms. For single-layer and bilayer graphene, the F_2G_2 model achieves accuracy near the K-point and away from it, capturing both the trigonal distortion of the bands near the K-point and the particle-hole symmetry breaking throughout the Brillouin zone [24]. Similarly, for MBN, the F_2G_2 model achieves accuracy near the K-point, as shown in the Fig. 3(b). Given that MBN exhibits low-energy band edges near K, the F_2G_2 model could serve as an alternative to the FTB model. In contrast, for BLBN with different stackings, the lower conduction band edge does not always lie at the K-point. In AB, AA', and AB' stackings, the conduction band edges are located at the M-point, resulting in an indirect bandgap. Conversely, AA and BA' stackings exhibit a direct bandgap, illustrated in Fig. 4. The bandgap nature and magnitude in these systems are illustrated in Fig. 3(d). The overall energy difference between the primary conduction band edges at the K-point and M-point for different stackings is approximately ± 400 meV, as indicated by the dashed blue line. Additionally a comprehensive overview is presented in Fig. 5 showing the surface plots of the lowest valence (VB₁) and conduction (CB₁) bands across the entire Brillouin zone, calculated using the FTB model.

While valence band maxima generally occur at the K points (except for AA'), valence band minima are consistently found at the Γ point. Interestingly, the AA' stacking shows valence band crossings at the K points. Regarding conduction bands, minima appear at the M point for most stackings but shift to the K point for AA and BA' configurations. The F_2G_2 effective model is unable to reproduce these features of bilayers.

As depicted in Fig. 6, the second coordination shell, represented by the pink large circle, comprises six intra-sublattice

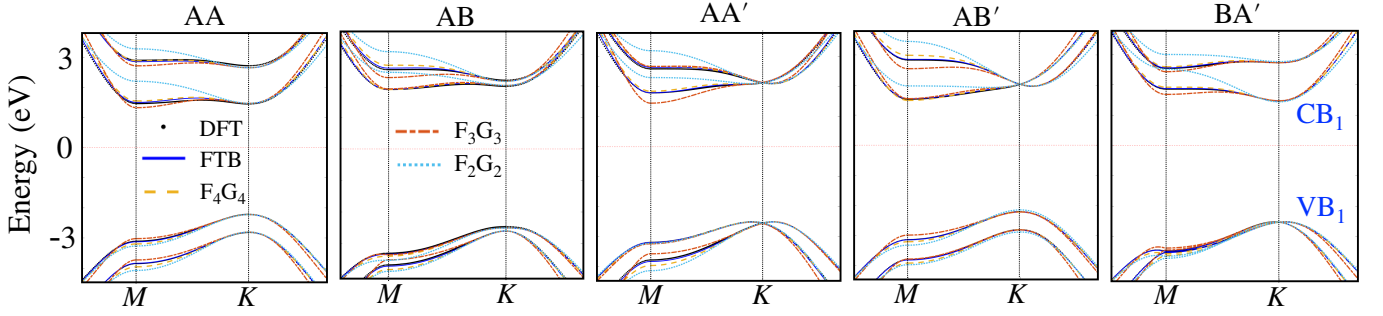


FIG. 4. (Color online) Comparison of the band structures for BLBN stackings (AA, AB, AA', AB', BA'), obtained from DFT and compared with the FTB and the simpler effective TB (F_2G_2 , F_3G_3 & F_4G_4) models. The accuracy of the FTB and F_4G_4 models in reproducing the *ab initio* π -bands along the specified k -path, compared to F_2G_2 and F_3G_3 models which deviate at the M -point, is shown. The primary valence and conduction bands are labeled as VB_1 and CB_1 , respectively, in the rightmost panel.

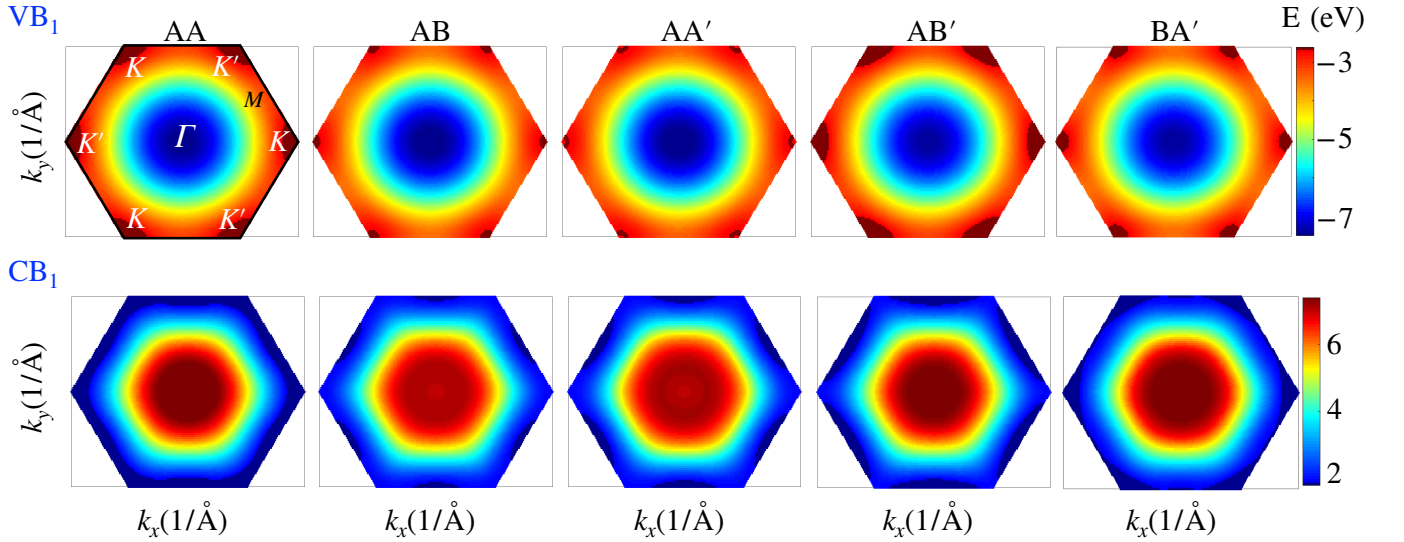


FIG. 5. (Color online) The surface plots of the primary bands VB_1 and CB_1 , calculated using the FTB model across the entire FBZ for various BLBN stackings, are depicted here. The letters in the top left panel denote the high symmetry points within the FBZ. It is observed that the VB_1 maxima occur at the K point (except for AA'), while the VB_1 minima are consistently found at the Γ point. The AA' stacking shows valence band crossings at the K point. The CB_1 minima appear at the M point for most stackings but shift to the K point for AA and BA' configurations.

(G_2) neighbors arranged in an alternating pattern (indicated by black and red arrows). For AB, AA' , AB' , and BA' stacked bilayers, the interlayer G_2 hopping energies between these alternating sublattices differ due to variations in the local atomic environment. The F_2G_2 model, with its limited number of hopping terms and assumption of equal interlayer G_2 hopping energies, fails to capture these subtle structural differences, leading to inaccuracies in the calculated band structure near the M -point. Therefore, there is a necessity for improved simplified TB models that can accurately capture the complex bandgap behavior of BLBN by effectively reproducing the low-energy bands near both the K and M points, matching the precision of the FTB model.

We further extended these models to include interactions with up to $n = 3$ and 4 nearest neighbors, denoted as F_3G_3 and F_4G_4 models, respectively. This inclusion improves the accuracy of the band structure, particularly at regions away

from the K -point. In these models, we incorporate *ab initio* hopping data for the shortest hopping terms, while correcting the most distant hopping terms using the following relations:

$$n = 3:$$

$$\begin{aligned} t_{\alpha\beta 3} &= 2C_{\alpha\beta 1}/\sqrt{3}a + t_{\alpha\beta 1} - 2t_{\alpha\beta 2}, \\ t'_{\alpha\beta 3} &= \frac{1}{3}(-C'_{\alpha\beta 0} + t'_{\alpha\beta 0} - 3t'_{\alpha\beta 1} + 6t'_{\alpha\beta 2}), \end{aligned} \quad (6)$$

$$n = 4:$$

$$\begin{aligned} t_{\alpha\beta 4} &= \frac{-1}{5}(2C_{\alpha\beta 1}/\sqrt{3}a + t_{\alpha\beta 1} - 2t_{\alpha\beta 2} - t_{\alpha\beta 3}), \\ t'_{\alpha\beta 4} &= \frac{1}{6}(-C'_{\alpha\beta 0} + t'_{\alpha\beta 0} - 3t'_{\alpha\beta 1} + 6t'_{\alpha\beta 2} - 3t'_{\alpha\beta 3}) \end{aligned} \quad (7)$$

The effective TB models with $n = 2$ and 3 neighbors successfully capture the crucial low-energy bands near the K -

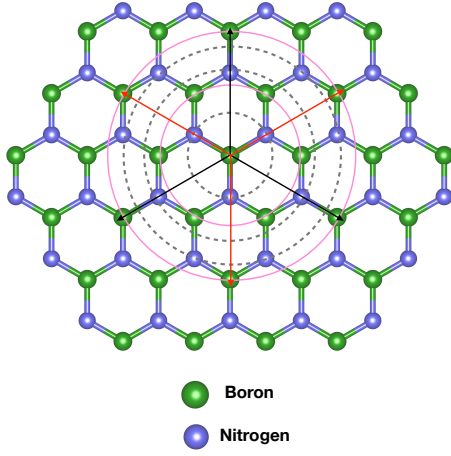


FIG. 6. (Color online) The nearest neighbor mapping in the TB models is illustrated. Dashed gray circles depict inter sublattice nearest neighbors, while solid pink circles show intra-sublattice nearest neighbors, with the central boron atom at the origin. The index n , representing the order of the nearest neighbor, increases with the radius of the circles.

point, including the presence or absence of band crossings for specific stacking configurations. However, their accuracy deviates from *ab initio* calculations, particularly away from the K -point. Remarkably, the F_4G_4 model reproduces the *ab initio* low-energy band edges near both the K -point and the M -point, demonstrating its superior ability to capture the electronic structure across the entire Brillouin zone. This makes the F_4G_4 model particularly valuable for detailed electronic structure analysis in h -BN systems. The limitations observed in the F_2G_2 model are mitigated in higher-order effective models, as evidenced by Tables B1 to B6. In these data tables, the four sub-lattices of bilayer h -BN, namely B_1 , N_1 , B_2 , and N_2 , are denoted by the labels A , B , A' , and B' , respectively. Supporting codes and data files used to generate the effective models presented in the tables and figures are accessible at [33].

C. Effect of strains

Further, to model the electronic properties of h -BN bilayers efficiently using the F_4G_4 model, we explored the impact of the lattice constant (a) on the effective hopping parameters. Specifically, we computed the hopping terms of the F_4G_4 TB model for various lattice constants of the bilayers. It is found that the nearest-neighbor hopping term ($n = 1$) shows significant variation, whereas the more distant ($n = 4$) effective hopping parameters remain largely consistent despite variations in the lattice constants across all hopping processes of each stacking configuration. We have presented the hopping parameters for specific lattice constant values around $a \sim 2.42$, 2.48, 2.51 Å for AB-stacked BLBN in Fig. 7(a) & (b). It is observed that, with a $\sim 1\%$ variation in a , the magnitude of the first nearest neighbor ($n = 1$) hopping energy changes by

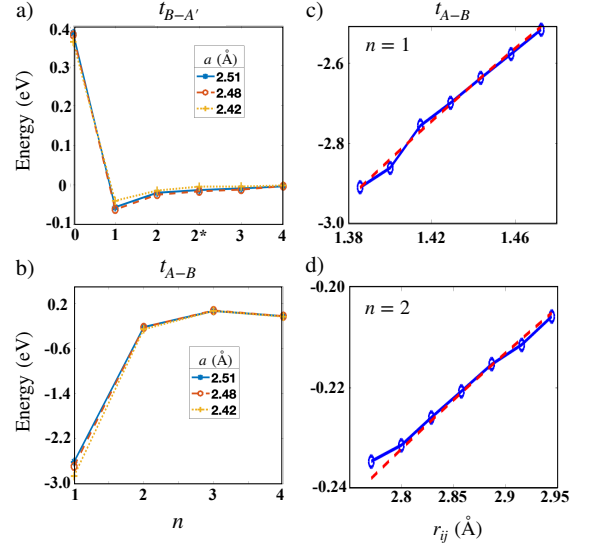


FIG. 7. (Color online) The hopping energies as a function of the nearest-neighbor index (n) for the AB-stacked BLBN are depicted for two processes: a) interlayer hopping from sublattice B to A' and b) intra-layer hopping from sublattice A to B . Different curves represent results obtained using various lattice constant values. The neighbor index n signifies the increasing distance between the interacting atoms, with $n = 2$ and 2^* indicating the interlayer G_2 processes depicted by red and black arrows, respectively, in Fig. 6. c) and d) illustrate the intra-layer hopping data t_{A-B} for nearest neighbors $n = 1$ and $n = 2$, respectively, as a function of bond length r_{ij} . The calculated data are shown in blue, while the fitting function, provided in Eq. (8), is depicted in red.

$\sim 3\%$ in the intra-layer A to B process (corresponding to G_n) and by $\sim 2\%$ in the interlayer B to A' process (corresponding to F_n). For understanding the effect of bond distortions on the Fermi velocity in BLBN systems, we have calculated the first nearest neighbor hopping energy for the intra-layer process between A -sublattice at site \mathbf{r}_i to the B -sublattice at site \mathbf{r}_j as a function of bond length, in the most stable AB-stacking. The hopping energy exhibits an exponential dependence on the bond length ($r_{ij} = |\mathbf{r}_{ij}|$), which we fit with the following relation:

$$t_{AB}(r_{ij}) = t_{AB}(r_{0,ij}) \exp\left(-2.45\left(\frac{r_{ij} - r_{0,ij}}{r_{0,ij}}\right)\right) \quad (8)$$

Here, $t_{AB}(r_{0,ij})$ is the hopping energy calculated at the equilibrium bond length $r_{0,ij} = 1.43$ Å, which is approximately equal to -2.7 eV. There is a good agreement between the hopping data and the fitting function of Eq. (8) as shown in Fig. 7(c) & (d). From the above relation one can account the hopping terms for the lattice constants close to the experimental values.

Additionally, to investigate the dependence of hopping terms on interlayer distances c , we computed the F_4G_4 TB model hopping data for all stacking configurations with interlayer distances ranging from $c = 3.1$ to 3.5 Å in steps of 0.1 Å. We fitted this data with an exponential function of the form:

$$t_i(c) = a_i e^{b_i c} + c_i e^{d_i c} \quad (9)$$

Here, $t_i(c)$ represents the hopping energy in eV as a function of the interlayer distance. The index i corresponds to the neighbor index n associated with G or F structure factors, ranging up to $n = 4$. Specifically, for G structure factor hopping processes, i ranges from 0 to 4, while for F structure factor, i ranges from 1 to 4. This fitting model applies to both intra-layer and interlayer hopping processes between intra- and inter-sublattices across all stackings examined in this study. The corresponding fitting parameters a_i , b_i , c_i , and d_i are detailed in Tables B7 to B11 in Appendix. B. In Fig. 8(a) and (b), we demonstrate the quality of this fitting for the interlayer (B to A') hopping process and the intra-layer (A to B) hopping process in the AB-stacking.

This fitting function is suitable for all the hopping processes including the distant neighbor terms having the energy of the order of 10^{-3} eV. Our fitting parametrization can accurately reproduce the F_4G_4 -TB model band structures, at any intermediate interlayer distance. For instance, at the intermediate value of $c = 3.261$ Å in the AB-stacking, the fitting function can produce hopping terms as accurate as those listed in Table. B3, and the resulting band structures are in close agreement, as compared in Fig. 8(c). The increasing interlayer distance leads to an increase in the energy separation between the primary and secondary bands. Specifically, in Fig. 8(d) & (e), the separation between the primary valence band VB_1 and primary conduction band CB_1 at the K -point is plotted as a function of interlayer distance, obtained from Eq. 9 for AB-stacking.

IV. DISTANCE-DEPENDENT TWO-CENTER APPROXIMATION FOR INTERLAYER HOPPING PROCESSES

The two-center (TC) approximation offers a generalized TB model approach for studying the electronic structures of twisted h -BN bilayers with diverse stacking configurations. This approach has proven successful in capturing the electronic properties of twisted bilayer graphene [26–29]. We present a revised TC approximation that goes beyond fitting DFT bands and incorporates insights from effective models, unlike previous approaches in BLBN [30, 31]. Our model builds on the FTB and the well-established F_4G_4 model for intra-layer interactions. We incorporate a distance-dependent approach for interlayer hopping, which aligns well with the DFT Hamiltonian at the K -point [32]. The distance-dependent interlayer hopping energy in this TC approximation [26–29] is defined as:

$$t(r_{ij}) = n_{ij,z}^2 V_{pp\sigma}(r_{ij}) + (1 - n_{ij,z}^2) V_{pp\pi}(r_{ij}) \quad (10)$$

Here, r_{ij} is the relative distance between two sublattices positioned at boron or nitrogen atoms from different layers, each

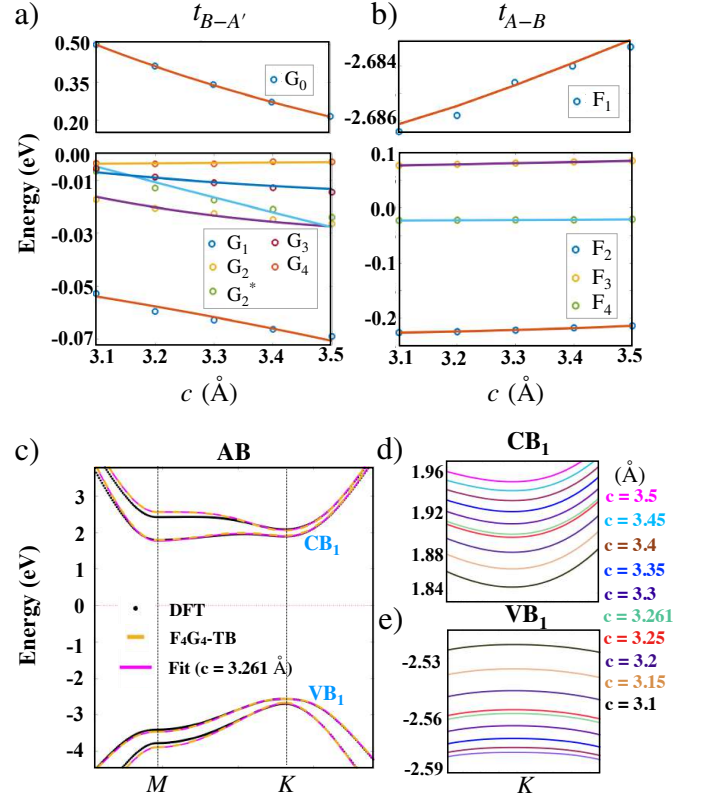


FIG. 8. (Color online) The hopping energy data fitting using Eq. (9) as a function of interlayer distance for AB-stacked BLBN is shown for two processes: a) interlayer hopping between B to A' and b) intra-layer hopping between A to B . Each curve represents different neighbor indices (n), with the data points denoted by circles. c) Comparison of the band structures for AB-stacked BLBN at $c = 3.261$ Å, showing results from DFT, the F_4G_4 -TB model, and the fitted F_4G_4 -TB model from Eq. (9). At the K -point, the separation between d) the primary conduction band CB_1 and e) the valence band VB_1 is illustrated for different values of c (Å).

located at \mathbf{r}_i and \mathbf{r}_j , respectively. The $n_{ij,z}$ is the direction cosine of \mathbf{r}_{ij} , defined as $n_{ij,z} = z_{ij}/r_{ij}$, where z_{ij} is the coordinate of \mathbf{r}_{ij} along the z -axis.

We have

$$\begin{aligned} V_{pp\sigma}(r_{ij}) &= \gamma_1 \exp(q\sigma(1 - \frac{r_{ij}}{c})), \\ V_{pp\pi}(r_{ij}) &= \gamma_0 \exp(q\pi(1 - \frac{r_{ij}}{a_{BN}})) \end{aligned} \quad (11)$$

and

$$\frac{q\sigma}{c} = \frac{q\pi}{a_{BN}} = \frac{\ln(\gamma'_0/\gamma_0)}{a_{BN} - a} \quad (12)$$

where we use the nearest neighbor interaction $\gamma_0 = -2.7$ eV within a plane and the second nearest neighbor interaction γ'_0 as $0.1\gamma_0$ [26]. The a_{BN} is the bond length between boron and nitrogen (1.43 Å) and a is the optimized lattice parameter (2.48 Å) within LDA. We consider a constant interlayer distance $c = 3.261$ Å, to keep the h -BN layer in the BLBN to

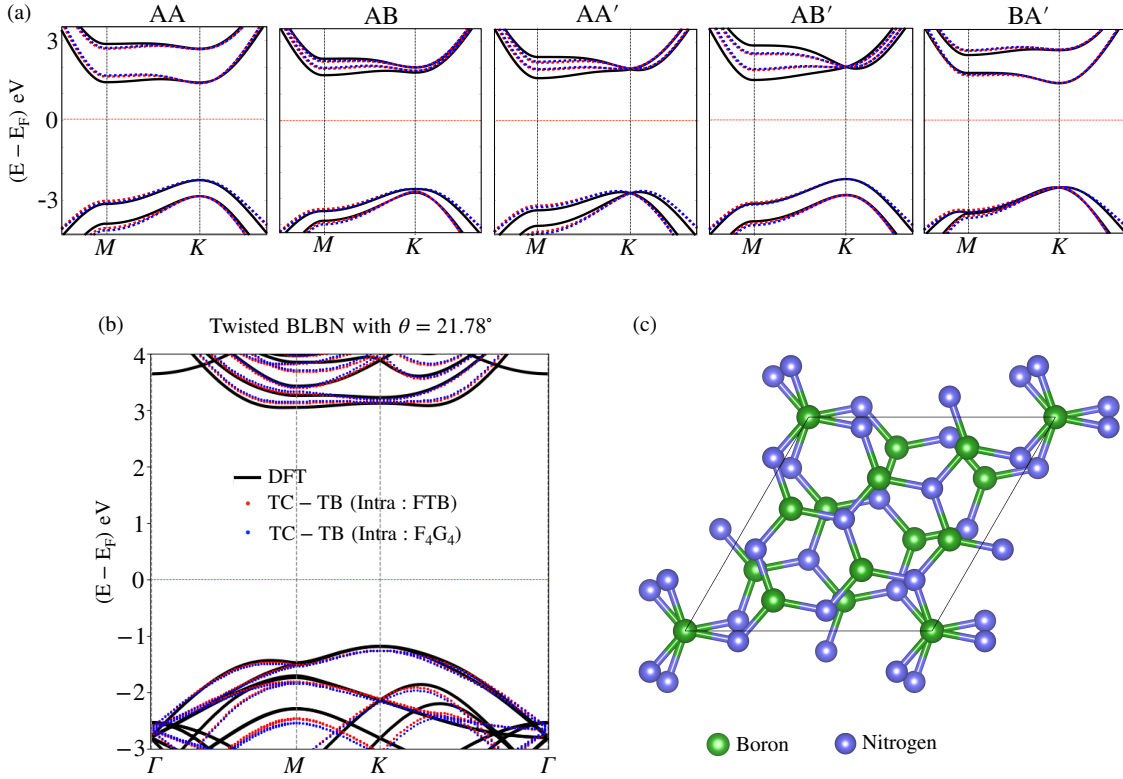


FIG. 9. (Color online) Comparison of bilayer hBN band structures obtained from DFT and with the TC-approximated TB model, incorporating both FTB and F_4G_4 models for intra-layer terms: (a) across all standard stackings of BLBN, (b) for a twisted BLBN configuration with $\theta = 21.78^\circ$, and (c) the schematic of the corresponding supercell.

be flat in these calculations. The prefactors of the interlayer hopping parameters for boron-boron, nitrogen-nitrogen, and boron-nitrogen interactions within the TC approximation are:

$$\begin{aligned} \gamma_{1,BB} &= 0.831 \text{ eV}, \\ \gamma_{1,NN} &= 0.3989 \text{ eV}, \\ \gamma_{1,BN} &= 0.6601 \text{ eV} \end{aligned} \quad (13)$$

The γ_1 terms are obtained by fitting the TB tunneling Hamiltonian element $H(K : \mathbf{d}_{xy})$ with *ab initio* data near the K -point [32]. Here, \mathbf{d}_{xy} represents the registry space of all possible in-plane relative positions for BLBN layers. This space encompasses all stackings achievable by translating one layer relative to the other within the range of $\mathbf{d}_x = 0$ to a and $\mathbf{d}_y = 0$ to $\sqrt{3}a$. This fitting process aims to minimize the error between the $H(K : \mathbf{d}_{xy})$ data obtained from both the TB model and LDA [27]. Substituting these values into Eqs. (10) to (12), we compute the interlayer hopping energies for various hopping processes within the BLBN system.

In Fig. 9 (a), we compare the band structures obtained from LDA calculations with those from the TC-approximated TB model (with intra-layer terms from FTB & F_4G_4) for various high symmetry stacking configurations of BLBN. The comparison reveals that our TC approximated TB model provides precise band dispersion near the K -point, comparable to DFT results. It effectively captures both crossing and non-crossing bands at the K -point for all standard stackings. However, it

lacks the accuracy away from the K -point.

Further, we calculated the band structure for a twisted BLBN supercell with $\theta = 21.78^\circ$, containing 28 atoms. This supercell was constructed using the optimized lattice constant $a = 2.48 \text{ \AA}$ and the equilibrium interlayer distance $c = 3.261 \text{ \AA}$ of AB-stacking. In Fig. 9(b), we compare the band structures of this twisted BLBN supercell, obtained using both LDA and the TC-approximated TB model, with intra-layer terms defined based on the AA-stacking configuration. Notably, our model shows close agreement with the DFT results. The close match between the bands plotted with red and blue dots, representing the FTB and F_4G_4 models used for intra-layer interactions, highlights a significant computational advantage of the F_4G_4 model. This advantage is especially pronounced for larger twisted BLBN supercells containing thousands of atoms, indicating that our model is a robust approach for accurately calculating the low-energy bands in such systems.

V. SUMMARY AND CONCLUSIONS

We present the development of π -band TB models for *h*-BN monolayer and bilayers by using maximally localized Wannier functions derived from DFT calculations of the electronic structure. We proposed three effective TB models as simplified alternatives to the complex 15-parameter FTB model. These models focus on accurately describing bands near the

high symmetry points (K and M) in the FBZ. Our analysis reveals that including hopping terms from up to $n = 4$ nearest neighbors (namely the F_4G_4 model) is necessary to capture the indirect nature of the DFT band gaps observed in various stacking configurations of bilayer h -BN. The limitation of the simpler F_2G_2 model ($n = 2$) stems from its limited number of hopping terms and the assumption of equal interlayer G_2 hopping parameters. Furthermore, we explore the influence of varying lattice parameters and interlayer distances on the effective hopping parameters in these systems to account for the effect of strains. Through fitting parameterization, we present an interlayer distance-dependent F_4G_4 model for each standard BLBN stacking type. In addition, we present a TC-approximated TB model that determines interlayer hopping parameters for any stacking or twisted configurations of BLBN. Our proposed model integrates the effective F_4G_4 and

FTB models for mapping intra-layer interactions, remains robust for calculating low-energy bands in twisted BLBN systems with many atoms per unit cell.

VI. ACKNOWLEDGEMENTS

This work was supported by the basic Study and Interdisciplinary R&D Fund of the University of Seoul (2022).

We acknowledge computational support from KISTI Grant No. KSC-2022-CRE-0514 and by the resources of Urban Big Data and AI Institute (UBAI) at UOS. J.J. also acknowledges support from the Korean Ministry of Land, Infrastructure and Transport (MOLIT) from the Innovative Talent Education Program for Smart Cities.

-
- [1] C. R. Dean, A. F. Young, I. Meric, C. Lee, L. Wang, S. Sorgenfrei, K. Watanabe, T. Taniguchi, P. Kim, K. L. Shepard, and J. Hone, Boron nitride substrates for high-quality graphene electronics, *Nat. Nanotechnol.* **5**, 722 (2010).
 - [2] J. Jung, A. Raoux, Z. Qiao, and A. H. MacDonald, *Ab initio* theory of moire superlattice bands in layered two-dimensional materials, *Phys. Rev. B* **89**, 205414 (2014).
 - [3] J. Jung, A. M. DaSilva, A. H. MacDonald, and S. Adam, Origin of band gaps in graphene on hexagonal boron nitride, *Nat. Commun.* **6**, 6308 (2015).
 - [4] M. Yankowitz, J. Xue, D. Cormode, J. D. Sanchez-Yamagishi, K. Watanabe, T. Taniguchi, P. Jarillo-Herrero, P. Jacquod, and B. J. LeRoy, Emergence of superlattice K -points in graphene on hexagonal boron nitride, *Nat. Phys.* **8**, 382 (2012).
 - [5] L. Xian, D. M. Kennes, N. Tancogne-Dejean, M. Altarelli, and A. Rubio, Multiflat Bands and Strong Correlations in Twisted Bilayer Boron Nitride: Doping-Induced Correlated Insulator and Superconductor, *Nano Lett.* **8**, 4934 (2019).
 - [6] X. Zhao, Y. Yang, D. Zhang, and S. Wei, Formation of Bloch Flat Bands in Polar Twisted Bilayers without Magic Angles, *Phys. Rev. B* **124**, 086401 (2020).
 - [7] P. Roman-Taboada, E. Obregon-Castillo, A. R. Botello-Mendez, and C. Noguez, Excitons in twisted AA' hexagonal boron nitride bilayers, *Phys. Rev. B* **108**, 075109 (2023).
 - [8] T. Galvani, F. Paleari, H. P. C. Miranda, A. Molina-Sánchez, L. Wirtz, S. Latil, H. Amara, and F. Ducastelle, Excitons in boron nitride single layer, *Phys. Rev. B* **94**, 125303 (2016).
 - [9] R. M. Ribeiro and N. M. R. Peres, Stability of boron nitride bilayers: Ground-state energies, interlayer distances, and tight-binding description, *Phys. Rev. B* **83**, 235312 (2011).
 - [10] F. Paleari, T. Galvani, H. Amara, F. Ducastelle, A. Molina-Sánchez, and L. Wirtz, Excitons in few-layer hexagonal boron nitride: Davydov splitting and surface localization, *2D Mater.* **5**, 045017 (2018).
 - [11] R. M. Ribeiro and N. M. R. Peres, Stability of boron nitride bilayers: Ground-state energies, interlayer distances, and tight-binding description, *Phys. Rev. B* **83**, 235312 (2011).
 - [12] D. Kim, Y. Lee, A. Chacón, D. Kim, Effect of Interlayer Coupling and Symmetry on High-Order Harmonic Generation from Monolayer and Bilayer Hexagonal Boron Nitride, *Symmetry* **14**, 84 (2022).
 - [13] S. Javvaji, J. H. Sun, and J. Jung, Topological flat bands without magic angles in massive twisted bilayer graphenes, *Phys. Rev. B* **101**, 125411 (2020).
 - [14] P. Giannozzi, S. Baroni, N. Bonini, M. Calandra, R. Car, C. Cavazzoni, D. Ceresoli, G. L. Chiarotti, M. Cococcioni, I. Dabo, A. Dal Corso, S. de Gironcoli, S. Fabris, G. Fratesi, R. Gebauer, U. Gerstmann, C. Gougousis, A. Kokalj, M. Lazzeri, L. Martin-Samos, N. Marzari, F. Mauri, R. Mazzarello, S. Paolini, A. Pasquarello, L. Paulatto, C. Sbraccia, S. Scandolo, G. Sclauzero, A. P. Seitsonen, A. Smogunov, P. Umari, and R. M. Wentzcovitch, Quantum ESPRESSO: a modular and open-source software project for quantum simulations of materials, *J. Phys.: Cond. Matter.* **21**, 395502 (2009).
 - [15] P. Giannozzi, O. Andreussi, T. Brumme, O. Bunau, M. B. Nardelli, M. Calandra, R. Car, C. Cavazzoni, D. Ceresoli, M. Cococcioni, and N. Colonna, I. Carnimeo, A. Dal Corso, S. de Gironcoli, P. Delugas, R.A. DiStasio, A. Ferretti, A. Floris, G. Fratesi, G. Fugallo, R. Gebauer, U. Gerstmann, F. Giustino, T. Gorni, J. Jia, M. Kawamura, H.-Y. Ko, A. Kokalj, E. Küçükbenli, M. Lazzeri, M. Marsili, N. Marzari, F. Mauri, N. L. Nguyen, H.-V. Nguyen, A. Otero-de-la-Roza, L. Paulatto, S. Poncé, D. Rocca, R. Sabatini, B. Santra, M. Schlipf, A. P. Seitsonen, A. Smogunov, I. Timrov, T. Thonhauser, P. Umari, N. Vast, X. Wu, and S. Baroni, Advanced capabilities for materials modelling with Quantum ESPRESSO, *J. Phys.: Cond. Matter.* **29**, 465901 (2017).
 - [16] D. Vanderbilt, Soft self-consistent pseudopotentials in a generalized eigenvalue formalism, *Phys. Rev. B* **41**, 7892–7895 (1990).
 - [17] J. P. Perdew and A. Zunger, Self-interaction correction to density-functional approximations for many-electron systems, *Phys. Rev. B* **23**, 5048–5079 (1981).
 - [18] R. W. Lynch and H. G. Drickamer, Effect of high pressure on the lattice parameters of diamond, graphite, and hexagonal boron nitride, *J. Chem. Phys.* **44**, 181 (1966).
 - [19] N. Marom, J. Bernstein, J. Garel, A. Tkatchenko, E. Joselevich, L. Kronik, and O. Hod, Stacking and registry effects in layered materials: the case of hexagonal boron nitride, *Phys. Rev. Lett.* **105**, 046801 (2010).
 - [20] G. Constantinescu, A. Kuc, and T. Heine, Stacking in bulk and bilayer hexagonal boron nitride, *Phys. Rev. Lett.* **111**, 036104 (2013).
 - [21] S. Latil, H. Amara and L. Sponza, Structural classification of

boron nitride twisted bilayers and ab initio investigation of their stacking-dependent electronic structure, *SciPost. Phys.* **14**, 053 (2023).

- [22] S. M. Gilbert, T. Pham, M. Dogan, S. Oh, B. Shevitski, G. Schumm, S. Liu, P. Ercius, S. Aloni, M. L. Cohen and A. Zettl, Alternative stacking sequences in hexagonal boron nitride, *2D Mater.* **6**, 021006 (2019).
- [23] N. Marzari, A. A. Mostofi, J. R. Yates, I. Souza, and D. Vanderbilt, Maximally localized Wannier functions: Theory and applications, *Rev. Mod. Phys.* **84**, 1419 (2012).
- [24] J. Jung and A. H. MacDonald, Tight-binding model for graphene π -bands from maximally localized Wannier functions, *Phys. Rev. B* **87**, 195450 (2013).
- [25] J. Jung and A. H. MacDonald, Accurate tight-binding models for the π bands of bilayer graphene, *Phys. Rev. B* **89**, 035405 (2014).
- [26] G. T. De Laissardiere, D. Mayou, and L. Magaud, Numerical studies of confined states in rotated bilayers of graphene, *Phys. Rev. B* **86**, 125413 (2012).
- [27] N. Leconte, S. Javvaji, J. An, A. Samudrala, and J. Jung, Relaxation effects in twisted bilayer graphene: A multiscale approach, *Phys. Rev. B* **106**, 115410 (2022).
- [28] N. N. T. Nam and M. Koshino, Lattice relaxation and energy band modulation in twisted bilayer graphene, *Phys. Rev. B* **96**, 075311 (2017).
- [29] G. T. De Laissardiere, D. Mayou, and L. Magaud, Localization of Dirac Electrons in Rotated Graphene Bilayers, *Nano Letters* **10**, 804 (2010).
- [30] P. Roman-Taboada, E. Obregon-Castillo, A. R. Botello-Mendez, and C. Noguez, Excitons in twisted AA' hexagonal boron nitride bilayers, *Phys. Rev. B* **108**, 075109 (2023).
- [31] L. Sponza, V. B. Vu, E. S. Richaud, H. Amara, and S. Latil, Emergence of flat bands in the quasicrystal limit of boron nitride twisted bilayers, (2024), arXiv:2310.02937 [cond-mat.mtrl-sci].
- [32] J. Jung, A. Raoux, Z. Qiao, and A. H. MacDonald, *Ab initio* theory of moiré superlattice bands in layered two-dimensional materials, *Phys. Rev. B* **89**, 205414 (2014).
- [33] The supporting codes and data files which are used to generate the figures in this paper are available at https://github.com/jsrivani/BNBN_Draft_files.

Appendix A: Taylor expansion of the Hamiltonian

The Taylor expansion of the Hamiltonian near the K -point can be expressed as:

$$H_{\alpha\beta}(\mathbf{k}_D + \mathbf{k}) = H_{\alpha\beta}(\mathbf{k}_D) + \left. \frac{\partial H_{\alpha\beta}}{\partial \mathbf{k}} \right|_{\mathbf{k}_D} \mathbf{k} + \frac{1}{2} \left. \frac{\partial^2 H_{\alpha\beta}}{\partial \mathbf{k}^2} \right|_{\mathbf{k}_D} \mathbf{k}^2 + \dots$$

For the intra-sublattice processes ($\alpha = \beta$), the first-order term (linear in \mathbf{k}) is negligible due to the symmetry operations inherent in the hexagonal lattice. These symmetries lead to a cancellation of contributions when summing over all equivalent positions within the unit cell. Therefore, we primarily consider the constant and quadratic terms. We define them as:

$$C'_{\alpha\beta 0} = H_{\alpha\alpha}(\mathbf{k}_D)$$

$$C'_{\alpha\beta 2} = \frac{1}{2} \left. \frac{\partial^2 H_{\alpha\alpha}}{\partial \mathbf{k}^2} \right|_{\mathbf{k}_D}$$

Thus, the Hamiltonian for intra-sublattice processes becomes:

$$H_{\alpha\beta}(\mathbf{k}_D + \mathbf{k}) \simeq C'_{\alpha\beta 0} + C'_{\alpha\beta 2} \mathbf{k}^2, \quad (\text{A1})$$

While the off-diagonal elements of the Hamiltonian, corresponding to inter-sublattice ($\alpha \neq \beta$) processes, include both linear and quadratic terms in \mathbf{k} with phase factors due to the angular dependence $\theta_{\mathbf{k}}$. The zeroth-order term is typically negligible because direct transitions between different sublattices without momentum transfer ($\mathbf{k} = 0$) are significantly reduced in amplitude. Thus, the relevant terms are:

$$C_{\alpha\beta 1} = \left. \frac{\partial H_{\alpha\beta}}{\partial \mathbf{k}} \right|_{\mathbf{k}_D}$$

$$C_{\alpha\beta 2} = \frac{1}{2} \left. \frac{\partial^2 H_{\alpha\beta}}{\partial \mathbf{k}^2} \right|_{\mathbf{k}_D}$$

The Hamiltonian for inter-sublattice processes becomes:

$$H_{\alpha\beta}(\mathbf{k}_D + \mathbf{k}) \simeq C_{\alpha\beta 1} \mathbf{k} e^{-i\theta_{\mathbf{k}}} + C_{\alpha\beta 2} \mathbf{k}^2 e^{i2\theta_{\mathbf{k}}}. \quad (\text{A2})$$

However, the zeroth-order expansion coefficient for intra-sublattice processes and the first-order expansion coefficient for inter-sublattice processes are essential for constructing the effective Hamiltonian and are derived from the hopping parameters [24]. They are given by:

$$C'_{\alpha\beta 0} = t'_0 - 3t'_1 + 6t'_2 - 3t'_3 - 6t'_4 + 6t'_5 + 6t'_6 - 6t'_7 \quad (\text{A3})$$

$$C_{\alpha\beta 1} = \frac{\sqrt{3}a}{2} (-t_1 + 2t_2 + t_3 - 5t_4 - 4t_5 + 7t_6 + 5t_7 + 2t_8 - 4t_9 + 11t_{10}) \quad (\text{A4})$$

Here, $t_n^{(\prime)} (= t_{\alpha\beta n}^{(\prime)})$ represents the hopping energy of the n^{th} nearest neighbor hopping process from sublattice α to β . The primes that are used both for the expansion coefficients and the hopping terms indicate that they involve expansions of G_n structure factor terms. The weights capture the contributions of the n -th hopping process. They are determined by symmetry considerations, including factors like atomic distances, the path orientation of the hopping process, and the phases of the wave functions involved.

Appendix B: Interlayer distance dependent fitting parametrization tables for F₄G₄-TB model in BLBN with stackings

In this section, we provide the data required for the c -dependent parametrization of the hopping energies in each

hopping process within the effective TB model with $n = 4$ for the BLBN system with different stackings. The hopping data obtained from first-principles, as a function of interlayer distance ranging from 3.1 to 3.5 Å for the given stackings, is fitted with a function described in Eq. (9). The fitting parameters for all the hopping processes in AA, AA', AB', BA', and AB stackings are listed in Tables B7, B8, B9, B10, and B11 below, respectively.

Monolayer <i>h</i> -BN				
F ₂ G ₂ model				
G _{<i>n</i>}	<i>t</i> _{AA}	<i>t</i> _{BB}	F _{<i>n</i>}	<i>t</i> _{AB}
G ₀	0.1648	-3.8678	F ₁	-2.7547
G ₁	0.0542	0.2228	F ₂	-0.1329
G ₂	0.0566	0.0429		
F ₃ G ₃ model				
G ₀	0.1648	-3.8678	F ₁	-2.7547
G ₁	0.0542	0.2228	F ₂	-0.2362
G ₂	0.0397	0.0329	F ₃	0.2068
G ₃	-0.0337	-0.0200		
F ₄ G ₄ model				
G ₀	0.1648	-3.8678	F ₁	-2.7547
G ₁	0.0542	0.2228	F ₂	-0.2362
G ₂	0.0397	0.0329	F ₃	0.0539
G ₃	-0.0361	-0.0250	F ₄	-0.0306
G ₄	0.0012	0.0025		

TABLE B1. The hopping parameters in eV units for MBN, used to construct the F₂G₂, F₃G₃, and F₄G₄ models, are listed here. The column labels F_{*n*} and G_{*n*} emphasize that they consist of the hopping terms related to the f_n and g_n structure factors, respectively, for the n^{th} nearest neighbor.

AA stacked BLBN							
F ₂ G ₂ model							
G _n	t _{AA}	t _{BB}	t _{AA'}	t _{BB'}	F _n	t _{AB}	t _{AB'}
G ₀	1.7666	-2.1843	0.7270	0.2705	F ₁	-2.7001	0.0265
G ₁	0.0053	0.1923	0.0498	-0.0185	F ₂	-0.1105	-0.0077
G ₂	0.0471	0.0370	0.0020	-0.0061			
F ₃ G ₃ model							
G ₀	1.7666	-2.1843	0.7270	0.2705	F ₁	-2.7001	0.0265
G ₁	0.0053	0.1923	0.0498	-0.0185	F ₂	-0.2102	0.0082
G ₂	0.0223	0.0195	0.0089	-0.0025	F ₃	0.1995	-0.0317
G ₃	-0.0497	-0.0351	0.0138	0.0072			
F ₄ G ₄ model							
G ₀	1.7666	-2.1843	0.7270	0.2705	F ₁	-2.7001	0.0265
G ₁	0.0053	0.1923	0.0498	-0.0185	F ₂	-0.2102	0.0082
G ₂	0.0223	0.0195	0.0089	-0.0025	F ₃	0.0797	-0.0176
G ₃	-0.0483	-0.0373	0.0139	0.0070	F ₄	-0.0240	0.0028
G ₄	-0.0007	0.0011	0.0000	0.0001			

TABLE B2. For AA-stacked BLBN, the hopping parameters in eV units used to construct the F₂G₂, F₃G₃, and F₄G₄ models are listed here. In the hopping processes of AA-stacking, $t_{A'A'} = t_{AA}$, $t_{B'B'} = t_{BB}$, $t_{A'B'} = t_{AB}$, and $t_{BA'} = t_{AB'}$ by symmetry relations. The column labels F_n and G_n emphasize that they consist of the hopping terms related to the f_n and g_n structure factors, respectively, for the n^{th} nearest neighbor.

AB stacked BLBN											
F ₂ G ₂ model											
G _n	t _{AA}	t _{BB}	t _{A'A'}	t _{B'B'}	t _{BA'}	F _n	t _{AB}	t _{A'B'}	t _{AA'}	t _{BB'}	t _{AB'}
G ₀	1.6636	-2.3393	1.7128	-2.2591	0.3809	F ₁	-2.6971	-2.7190	0.4841	-0.0176	0.1209
G ₁	0.0235	0.1903	0.0108	0.1910	-0.0617	F ₂	-0.1248	-0.1129	0.0457	-0.0545	-0.1437
G ₂	0.0496	0.0388	0.0490	0.0328	-0.0158						
F ₃ G ₃ model											
G ₀	1.6636	-2.3393	1.7128	-2.2591	0.3809	F ₁	-2.6971	-2.7190	0.4841	-0.0176	0.1209
G ₁	0.0235	0.1903	0.0108	0.1910	-0.0617	F ₂	-0.2207	-0.2044	0.0743	-0.0472	-0.1387
G ₂	0.0274	0.0212	0.0257	0.0148	-0.0245	F ₃	0.1917	0.1829	-0.0573	-0.0146	-0.0099
G ₂ [*]	0.0274	0.0212	0.0257	0.0148	-0.0159						
G ₃	-0.0446	-0.0352	-0.0466	-0.0359	-0.0175						
F ₄ G ₄ model											
G ₀	1.6636	-2.3393	1.7128	-2.2591	0.3809	F ₁	-2.6971	-2.7190	0.4841	-0.0176	0.1209
G ₁	0.0235	0.1903	0.0108	0.1910	-0.0617	F ₂	-0.2207	-0.2044	0.0743	-0.0472	-0.1387
G ₂	0.0274	0.0212	0.0257	0.0148	-0.0245	F ₃	0.0779	0.0795	0.0520	0.0207	-0.0215
G ₂ [*]	0.0274	0.0212	0.0257	0.0148	-0.0159	F ₄	-0.0228	-0.0207	0.0219	0.0071	-0.0023
G ₃	-0.0419	-0.0367	-0.0441	-0.0372	-0.0116						
G ₄	-0.0013	0.0007	-0.0012	0.0007	-0.0030						

TABLE B3. For AB-stacked BLBN, the hopping parameters in eV units used to construct the F₂G₂, F₃G₃, and F₄G₄ models are listed here. The column labels F_n and G_n emphasize that they consist of the hopping terms related to the f_n and g_n structure factors, respectively, for the n^{th} nearest neighbor.

AA' stacked BLBN									
F ₂ G ₂ model									
G _n	<i>t</i> _{AA}	<i>t</i> _{BB}	<i>t</i> _{A'A'}	<i>t</i> _{B'B'}	<i>t</i> _{AA'}	F _n	<i>t</i> _{AB}	<i>t</i> _{AB'}	<i>t</i> _{BA'}
G ₀	1.6717	−2.3068	−2.3074	1.6716	0.4310	F ₁	−2.7049	0.4239	−0.0613
G ₁	0.0122	0.1900	0.1900	0.0122	−0.0684	F ₂	−0.1176	0.1338	−0.0161
G ₂	0.0520	0.0372	0.0372	0.0520	−0.0344				
F ₃ G ₃ model									
G ₀	1.6717	−2.3068	−2.3074	1.6716	0.4310	F ₁	−2.7049	0.4239	−0.0613
G ₁	0.0122	0.1900	0.1900	0.0122	−0.0684	F ₂	−0.2136	0.1798	0.0031
G ₂	0.0288	0.0186	0.0186	0.0288	−0.0415	F ₃	0.1921	−0.0919	−0.0383
G ₂ [*]	0.0288	0.0186	0.0186	0.0288	−0.0163				
G ₃	−0.0463	−0.0370	−0.0370	−0.0463	−0.0142				
F ₄ G ₄ model									
G ₀	1.6717	−2.3068	−2.3074	1.6716	0.4310	F ₁	−2.7049	0.4239	−0.0613
G ₁	0.0122	0.1900	0.1900	0.0122	−0.0684	F ₂	−0.2136	0.1798	0.0031
G ₂	0.0288	0.0186	0.0186	0.0288	−0.0415	F ₃	0.0803	0.0261	0.0121
G ₂ [*]	0.0288	0.0186	0.0186	0.0288	−0.0163	F ₄	−0.0224	0.0236	0.0101
G ₃	−0.0438	−0.0381	−0.0381	−0.0438	−0.0072				
G ₄	−0.0013	0.0005	0.0005	−0.0013	−0.0035				

TABLE B4. For AA'-stacked BLBN, the hopping parameters in eV units used to construct the F₂G₂, F₃G₃, and F₄G₄ models are listed here. In the hopping processes of AA'-stacking, $t_{BB'} = t_{AA'}$ and $t_{A'B'} = t_{AB}$ by symmetry relations. The column labels F_n and G_n emphasize that they consist of the hopping terms related to the f_n and g_n structure factors, respectively, for the n^{th} nearest neighbor.

AB' stacked BLBN							
F ₂ G ₂ model							
G _n	t _{AA}	t _{BB}	t _{BA'}	F _n	t _{AB}	t _{AA'}	t _{AB'}
G ₀	1.8176	-2.1740	0.2059	F ₁	-2.6892	0.0687	0.4460
G ₁	0.0183	0.1911	-0.0283	F ₂	-0.1183	-0.0823	-0.0686
G ₂	0.0451	0.0377	0.0129				
F ₃ G ₃ model							
G ₀	1.8176	-2.1740	0.2059	F ₁	-2.6892	0.0687	0.4460
G ₁	0.0183	0.1911	-0.0283	F ₂	-0.2104	-0.0771	-0.0328
G ₂	0.0219	0.0205	0.0170	F ₃	0.1842	-0.0103	-0.0717
G ₂ [*]	0.0219	0.0205	-0.0064				
G ₃	-0.0464	-0.0343	0.0083				
F ₄ G ₄ model							
G ₀	1.8176	-2.1740	0.2059	F ₁	-2.6892	0.0687	0.4460
G ₁	0.0183	0.1911	-0.0283	F ₂	-0.2104	-0.0771	-0.0328
G ₂	0.0219	0.0205	0.0170	F ₃	0.0752	-0.0054	0.0452
G ₂ [*]	0.0219	0.0205	-0.0064	F ₄	-0.0218	0.0010	0.0234
G ₃	-0.0431	-0.0356	0.0063				
G ₄	-0.0016	0.0007	0.0010				

TABLE B5. For AB'-stacked BLBN, the hopping parameters in eV units used to construct the F₂G₂, F₃G₃, and F₄G₄ TB models are listed here. In the hopping processes of AB'-stacking, $t_{A'A'} = t_{BB}$, $t_{B'B'} = t_{AA}$, $t_{A'B'} = t_{AB}$, and $t_{BB'} = t_{AA'}$ by symmetry relations. The column labels F_n and G_n emphasize that they consist of the hopping terms related to the f_n and g_n structure factors, respectively, for the n^{th} nearest neighbor.

BA'-stacked BLBN							
F ₂ G ₂ model							
G _n	t _{AA}	t _{BB}	t _{AB'}	F _n	t _{AB}	t _{AA'}	t _{BA'}
G ₀	1.8325	-2.1688	0.7813	F ₁	-2.6866	0.0763	0.0604
G ₁	0.0096	0.1965	0.0877	F ₂	-0.1202	-0.0569	-0.0735
G ₂	0.0497	0.0379	0.0242				
F ₃ G ₃ model							
G ₀	1.8325	-2.1688	0.7813	F ₁	-2.6866	0.0762	0.0604
G ₁	0.0096	0.1965	0.0877	F ₂	-0.2187	-0.0622	-0.0665
G ₂	0.0244	0.0204	0.0312	F ₃	0.1971	0.0106	-0.0140
G ₂ *	0.0244	0.0204	0.0193				
G ₃	-0.0507	-0.0352	0.0140				
F ₄ G ₄ model							
G ₀	1.8325	-2.1688	0.7813	F ₁	-2.6866	0.0763	0.0604
G ₁	0.0096	0.1965	0.0877	F ₂	-0.2187	-0.0622	-0.0665
G ₂	0.0244	0.0204	0.0312	F ₃	0.0794	-0.0141	0.0122
G ₂ *	0.0244	0.0204	0.0193	F ₄	-0.0235	-0.0049	0.0052
G ₃	-0.0466	-0.0370	0.0093				
G ₄	-0.0020	0.0009	0.0024				

TABLE B6. For BA'-stacked BLBN, the hopping parameters in eV units used to construct the F₂G₂, F₃G₃, and F₄G₄ TB models are listed here. In the hopping processes of BA'-stacking, $t_{A'A'} = t_{BB}$, $t_{B'B'} = t_{AA}$, $t_{A'B'} = t_{AB}$, and $t_{BB'} = t_{AA'}$ by symmetry relations. The column labels F_n and G_n emphasize that they consist of the hopping terms related to the f_n and g_n structure factors, respectively, for the n^{th} nearest neighbor.

	A - A	B - B	A - A'	B - B'	A - B	A - B'
a ₀	0.4606	-4.0140	2.2170	1.6800	-	-
b ₀	0.3915	-0.1848	-2.7200	-0.1375	-	-
c ₀	0.0256	-0.0024	1.4480	-0.2480	-	-
d ₀	0.4038	-4.6280	-0.2130	0.3563	-	-
a ₁	-0.0093	0.6383	-0.3910	-0.1087	-0.9425	1.9030
b ₁	0.6518	0.1833	0.6001	0.1701	-8.8350	-0.9914
c ₁	0.0055	-0.4867	0.3238	0.0715	-2.9180	-0.0007
d ₁	0.8256	0.2112	0.6629	0.2693	-0.0238	1.2810
a ₂	-0.0002	0.0268	0.0202	0.0095	-0.1598	8.8100
b ₂	0.6784	0.4281	0.7543	0.3499	0.0820	-2.8300
c ₂	0.0040	-0.0191	-0.0403	-0.0157	9.2690	1.3430
d ₂	0.5384	0.4734	0.5324	0.2181	-7.2540	-1.5260
a ₃	0.5653	0.0108	0.1714	0.4662	0.0015	-0.1925
b ₃	-0.2976	0.5824	-0.1436	0.7221	-1.2870	-0.0979
c ₃	-0.6604	-0.0367	-0.3223	-0.4688	0.0782	0.4838
d ₃	-0.2825	0.3377	-0.3789	0.7200	0.0111	-0.4207
a ₄	-0.0077	-0.0005	-0.0725	0.0002	-0.0454	-0.1698
b ₄	0.5426	-9.3350	-0.6360	0.8318	-0.1396	0.1638
c ₄	0.0072	0.0010	0.0065	-0.0006	0.0214	0.2067
d ₄	0.5580	0.0058	0.0999	0.4771	-0.2948	0.1068

TABLE B7. The fitting parameters a_i , b_i , c_i , and d_i for the c -dependent hopping parametrization shown in Eq. (9), for the F₄G₄ model for AA-stacked BLBN are presented. Here, i represents the neighbor index n . The top row of the table illustrates the hopping processes between corresponding sublattices. In AA-stacking, $t_{A'A'} = t_{AA}$, $t_{B'B'} = t_{BB}$, $t_{A'B'} = t_{AB}$, and $t_{BA'} = t_{AB'}$ by symmetry relations. The hopping parameters are given in eV units.

	$A - A$	$B - B$	$A - A'$	$A - B$	$A - B'$	$B - A'$
a_0	0.0164	0.4819	2.8020	-	-	-
b_0	-3.0860	0.2315	-0.3861	-	-	-
c_0	1.5040	-1.7470	-0.0073	-	-	-
d_0	0.0303	0.1979	1.1910	-	-	-
a_1	-0.0931	0.3269	-0.0279	-2.4920	-5.4770	-0.8401
b_1	-0.2723	-0.1689	0.2853	-9.2210	-6.0280	0.2899
c_1	11.750	-1.7430	7.1910	-2.6770	1.8530	0.6791
d_1	-1.6680	-7.4570	-9.0300	0.0038	-0.4450	0.3461
a_2	0.3006	3.9530	0.9573	0.0056	-0.2072	1.0550
b_2	0.3349	-1.0680	0.1134	-0.0310	-0.3630	0.1763
c_2	-0.2654	-4.3010	-0.9907	-0.4010	0.6907	-1.1360
d_2	0.3630	-1.1420	0.1122	-0.1920	-0.3184	0.1531
a_2^*	0.3006	3.9530	0.2170	-	-	-
b_2^*	0.3349	-1.0680	0.4179	-	-	-
c_2^*	-0.2654	-4.3010	-0.2164	-	-	-
d_2^*	0.3630	-1.1420	0.4246	-	-	-
a_3	-0.0187	-0.0178	-0.0703	0.0285	0.1277	0.9009
b_3	0.2587	0.2275	0.3113	0.3129	0.2866	0.5398
c_3	-0.0838	-0.6783	0.0801	0.0061	-0.1503	-0.9120
d_3	-1.8550	-9.6650	0.2584	-10.520	0.2081	0.5353
a_4	0.1765	0.0204	0.1122	0.0183	0.0147	0.0028
b_4	0.3853	-1.1480	-0.1774	-9.8800	0.0422	0.3726
c_4	-0.1565	0.1483	-0.1163	-0.0536	0.0046	-3.7130
d_4	0.4226	-3.4070	-0.1702	-0.2787	0.1945	-4.746

TABLE B8. The fitting parameters a_i , b_i , c_i , and d_i for the c -dependent hopping parametrization shown in Eq. (9), for the F_4G_4 model for AA' -stacked BLBN are presented. Here, i represents the neighbor index n . The top row of the table illustrates the hopping processes between corresponding sublattices. In AA' -stacking, $t_{A'A'} = t_{BB}$, $t_{B'B'} = t_{AA}$, $t_{A'B'} = t_{AB}$, and $t_{BB'} = t_{AA'}$ by symmetry relations. The hopping parameters are given in eV units.

	$A-A$	$B-B$	$B-A'$	$A-B$	$A-A'$	$A-B'$
a_0	0.9895	-0.1395	0.8377	-	-	-
b_0	0.2307	-4.9030	-0.0721	-	-	-
c_0	-0.0034	-2.2510	-0.0643	-	-	-
d_0	1.3550	-0.0105	0.5943	-	-	-
a_1	4.1740	1.2190	-0.2888	1.8790	3.9740	-0.0145
b_1	-1.6680	-6.9440	-5.5960	-9.1540	-0.7872	0.6848
c_1	0.1304	0.2440	-10.570	-2.7100	-0.4307	1.0160
d_1	-4.5090	-0.0753	-1.8350	-0.0023	-0.1839	-0.1714
a_2	-0.0037	-0.0112	0.0840	-0.3066	-0.0613	0.0646
b_2	0.7808	0.7136	-9.7680	-0.1052	0.0712	0.1191
c_2	0.0104	0.0235	0.0011	8.1740	-2.8940	-14.240
d_2	0.5810	0.5375	0.8206	-2.1490	-7.2330	-1.4450
a_2^*	-0.0037	-0.0112	-0.5739	-	-	-
b_2^*	0.7808	0.7136	0.3430	-	-	-
c_2^*	0.0104	0.0235	0.5383	-	-	-
d_2^*	0.5810	0.5375	0.3615	-	-	-
a_3	0.0469	7.2940	-0.0343	0.0312	5.2910	-1.3750
b_3	-4.1440	-9.0010	0.6859	0.2687	-1.7530	0.5064
c_3	-0.0225	-0.0157	0.0310	0.0000	-0.0022	1.3750
d_3	0.1979	0.2507	0.7234	-10.900	0.7159	0.5083
a_4	0.2959	0.0045	0.0065	-0.0324	0.4313	-0.0016
b_4	-1.0540	-0.2546	-0.2343	-0.1242	0.2359	0.6225
c_4	-0.1077	-0.0004	-2.2330	2.5360	-0.3990	0.0171
d_4	-0.6937	0.3998	-2.1300	-12.150	0.2594	0.2214

TABLE B9. The fitting parameters a_i , b_i , c_i , and d_i for the c -dependent hopping parametrization shown in Eq. (9), for the F_4G_4 model for AB' -stacked BLBN are presented. Here, i represents the neighbor index n . The top row of the table illustrates the hopping processes between corresponding sublattices. In AB' -stacking, $t_{A'A'} = t_{BB}$, $t_{B'B'} = t_{AA}$, $t_{A'B'} = t_{AB}$, and $t_{BB'} = t_{AA'}$ by symmetry relations. The hopping parameters are given in eV units.

	$A-A$	$B-B$	$A-B'$	$A-B$	$A-A'$	$B-A'$
a_0	1.7450	-0.4610	-1.0390	-	-	-
b_0	0.4394	0.4089	0.7784	-	-	-
c_0	-0.8599	-60.580	1.3910	-	-	-
d_0	0.5683	-1.5240	0.7067	-	-	-
a_1	0.2493	0.0759	-0.0556	-2.6490	3.6570	8.0410
b_1	0.4731	0.1196	1.1320	0.0043	-0.7636	-0.1605
c_1	-0.2362	0.2223	0.0465	0.3333	-0.1874	-7.0360
d_1	0.4874	-0.3001	1.1980	-2.4060	0.05863	-0.1236
a_2	0.0634	0.3877	0.0002	-0.2814	0.1185	5.5470
b_2	0.3311	-0.1194	1.4740	-0.0789	-9.8480	-2.3650
c_2	-0.0482	-0.3550	0.0000	0.0000	-0.0280	-3.0960
d_2	0.3728	-0.1166	-9.9250	-15.660	0.2427	-1.1660
a_2^*	0.0634	0.3877	-0.0779	-	-	-
b_2^*	0.3311	-0.1194	0.4572	-	-	-
c_2^*	-0.0482	-0.3550	0.0682	-	-	-
d_2^*	0.3728	-0.1166	0.5146	-	-	-
a_3	-0.1957	0.0062	-0.3733	-1.7680	0.4363	0.0000
b_3	-0.6550	0.1607	-0.4989	-7.6770	-0.4018	-14.260
c_3	-0.0027	-0.0306	0.1213	0.0595	-0.1385	0.0002
d_3	0.6550	0.1345	-0.1180	0.0894	-0.0170	1.2130
a_4	-0.0725	0.1227	0.0550	2.2160	-0.0660	0.4512
b_4	-1.1070	-1.5420	0.4468	-10.750	0.4113	-0.0064
c_4	0.9846	0.0000	-0.0619	-0.0282	0.0908	-0.4692
d_4	-4.0320	-13.8600	0.4074	-0.0593	0.3079	-0.0221

TABLE B10. The fitting parameters a_i , b_i , c_i , and d_i for the c -dependent hopping parametrization shown in Eq. (9), for the F_4G_4 model for BA' -stacked BLBN are presented. Here, i represents the neighbor index n . The top row of the table illustrates the hopping processes between corresponding sublattices. In BA' -stacking, $t_{A'A'} = t_{BB}$, $t_{B'B'} = t_{AA}$, $t_{A'B'} = t_{AB}$, and $t_{BB'} = t_{AA'}$ by symmetry relations. The hopping parameters are given in eV units.

	$A-A$	$B-B$	$A'-A'$	$B'-B'$	$B-A'$	$A-B$	$A'-B'$	$A-A'$	$B-B'$	$A-B'$
a_0	1.4020	0.0108	2.5140	0.0783	-0.0400	-	-	-	-	-
b_0	0.0526	0.6491	-6.3220	0.9919	0.3796	-	-	-	-	-
c_0	-0.0988	-2.5820	3.6710	-0.7260	42.640	-	-	-	-	-
d_0	-9.7670	-0.0221	-0.2225	0.5373	-1.359	-	-	-	-	-
a_1	1.4180	-0.0553	-0.1604	0.3536	-0.0059	-2.8050	-0.0222	-0.5973	-0.1576	-0.0386
b_1	-0.0319	0.1875	0.0707	-0.1884	0.7141	-0.0033	-4.3200	0.9163	-0.3161	0.3746
c_1	-1.2310	0.3135	0.2551	0.8459	4.2250	0.0924	-2.6880	0.7005	1.3570	9.9740
d_1	0.0069	-0.0232	-0.0568	-4.8530	-8.9810	-0.0101	0.0012	0.8792	-1.0680	-1.1130
a_2	0.5976	0.1805	-0.1176	-0.0004	-0.5243	-2.8900	0.7870	-0.6613	0.0008	-0.2680
b_2	-0.8391	-0.6548	0.3172	1.4970	-0.5917	-7.4550	-0.2730	0.8112	0.8209	-0.2156
c_2	-54.380	-0.0378	0.1424	0.0025	5.0960	-0.3349	-0.9677	0.6552	-0.1054	-0.9209
d_2	-2.5620	-1.4540	0.2810	1.0030	-1.3950	-0.1262	-0.1840	0.8161	-0.1697	-6.4990
a_2^*	0.5976	0.1805	-0.1176	-0.0004	0.4423	-	-	-	-	
b_2^*	-0.8391	-0.6548	0.3172	1.4970	-0.2127	-	-	-	-	
c_2^*	-54.3800	-0.0378	0.1424	0.0025	-0.2044	-	-	-	-	
d_2^*	-2.5620	-1.4540	0.2810	1.0030	0.0444	-	-	-	-	
a_3	0.0000	-0.0798	0.0000	-0.2003	-0.7780	0.0381	0.0364	-0.0089	0.1372	-0.5453
b_3	-18.650	-0.8135	-13.680	-0.9921	-0.6396	0.2253	0.2405	0.6663	0.2613	-0.2354
c_3	-0.0207	-0.0073	-0.0273	-0.0036	1.6600	-1.9910	-4.233	0.0128	-0.1557	1.4150
d_3	0.2181	0.4485	0.1478	0.6417	-0.9052	-7.3900	-5.304	0.7016	0.2034	-0.5496
a_4	-4.3320	0.2453	-4.0280	0.0421	0.0155	0.2825	-0.5826	0.0097	0.0026	-0.6390
b_4	-7.4290	-1.4510	-3.7300	0.1121	-10.720	0.0066	0.4629	0.2387	0.3089	-2.7570
c_4	-0.0005	-0.0968	-0.0003	-0.0377	-0.0132	-0.3180	0.5664	0.7201	-1.8140	4.0990
e_4	0.3698	-1.2520	0.4917	0.1420	-0.4014	-0.0066	0.4690	-3.8410	-5.5240	-3.9340

TABLE B11. The fitting parameters a_i , b_i , c_i , and d_i for the c -dependent hopping parametrization shown in Eq. (9), for the F_4G_4 model for AB-stacked BLBN are presented. Here, i represents the neighbor index n . The top row of the table illustrates the hopping processes between corresponding sublattices. The hopping parameters are given in eV units.